Observation of Bulk Defects by Scanning Tunneling Microscopy and Spectroscopy: Arsenic Antisite Defects in GaAs

R. M. Feenstra, J. M. Woodall, and G. D. Pettit
IBM Research Division, T. J. Watson Research Center, Yorktown Heights, New York 10598
(Received 28 April 1993)

The scanning tunneling microscope is used to study arsenic-related point defects in low-temperature-grown GaAs. Tunneling spectroscopy reveals a band of donor states located near $E_v+0.5$ eV arising from the defects. Images of this state reveal a central defect core, with two satellites located about 15 Å from the core. The structure of the defect is found to be consistent with that of an isolated arsenic antisite defect (As on a Ga site) in a tetrahedral environment.

PACS numbers: 61.16.Ch, 61.72.Ji, 71.55.Eq

The ability of the scanning tunneling microscope (STM) to resolve geometric structure on the atomic scale, while also providing electronic spectroscopy, has led to its wide applicability to problems involving both ordered and disordered surface structures. However, one area in which the STM has found relatively little application is in the study of *bulk* defects, that is, defects which are grown into the bulk of the material and thus are not surface specific [1]. Two reasons for this dearth of activity are that the number of bulk defects seen on a surface is generally quite low, and that surface reconstructions will often act to mask the presence of such defects. The first problem can be alleviated by using specially prepared material containing a very high density of defects, such as the low-temperature-grown (LT) GaAs used in the present work which contains about 1×10^{20} cm^{-3} arsenic-related point defects [2]. The second difficulty is avoided on the (110) cleavage face of GaAs, in which no reconstruction occurs (other than the well-known buckling of the surface) and the surface dangling bonds lie in energy outside of the band gap region. These favorable properties of the GaAs(110) surface have been used to advantage in numerous STM studies, including cross-sectional studies of thin layers grown by molecular-beam epitaxy (MBE) [3–5]. As demonstrated here for the first time, STM measurements can directly yield the energy levels and electronic structure of point defects—this information is especially significant for deep level defects and defect complexes, whose structure is generally difficult to discern by other techniques.

In this work, thin layers of LT GaAs are studied by cleaving the MBE-grown wafers in ultrahigh vacuum and viewing the layers in cross section. Tunneling spectroscopy reveals a band of donor states located near $E_v+0.5$ eV, arising from arsenic-related point defects in the material. Images of these states reveal four types of structures. The structures are all interpreted as belonging to the same type of defect, with the variation arising from the location of the defect relative to the cleavage plane. The images consist of a central defect core, with two satellites located about 15 Å from the core. Based on the observed number, symmetry, and spectroscopic properties of the defects, it is concluded that they consist of an isolated arsenic antisite (As on a Ga site), which is believed to be the dominant point defect in the material [2]. The observed satellites are interpreted as antisite wavefunction tails extending along ⟨112⟩ surface directions.

The LT GaAs layers, typically 1000 Å thick, were grown in a Varian Gen-II MBE system at a growth temperature of 225 °C. A cap layer grown at 350 °C was grown on top of the LT layer, and no subsequent annealing of the samples was performed. In addition to the 1×10^{20} cm^{-3} deep donor arsenic-related defects contained in the material, shallow donors or acceptors were also intentionally introduced. Three samples discussed here have shallow dopant concentrations of $n^+(1\times10^{19}$ cm^{-3} Si), $p^+(1\times10^{19}$ cm^{-3} Be), and $p^{++}(5\times10^{19}$ cm^{-3} Be). The samples are cleaved in the STM ultrahigh-vacuum chamber with a pressure of $<4\times10^{-11}$ Torr. Single-crystal ⟨111⟩-oriented tungsten probe tips are used. Prior to use they are thoroughly cleaned by electron-bombardment heating, and characterized by field-emission microscopy. Descriptions of the STM design, and spectroscopic methods, have been given previously [4,5].

Before presenting STM images of the arsenic-related defects, we first discuss tunneling spectroscopy results. Figure 1 shows typical spectra acquired from each of the three types of samples described above (at least two samples of each doping type have been studied, and good reproducibility is found). The spectra reveal tunneling out of valence-band states at large negative voltages and into conduction-band states at large positive voltages, with the band edges denoted by E_v and E_c, respectively. These bands are separated by the bulk band gap of 1.43 eV. On a region of the LT layer, which is *not* on a point defect, the spectra reveal zero current and conductance within the gap. If the probe tip is positioned on top of a point defect, then the spectra reveal large peaks within the gap region as seen in Fig. 1. Focusing first on Fig. 1(a), we find a band of states centered near $E_v+0.5$ eV, and the Fermi level (0 V) is located above this band. The location of this band is close to that for the donor states of an arsenic antisite defect (the upper state is the well-

0031-9007/93/71(8)/1176(4)$06.00
© 1993 The American Physical Society

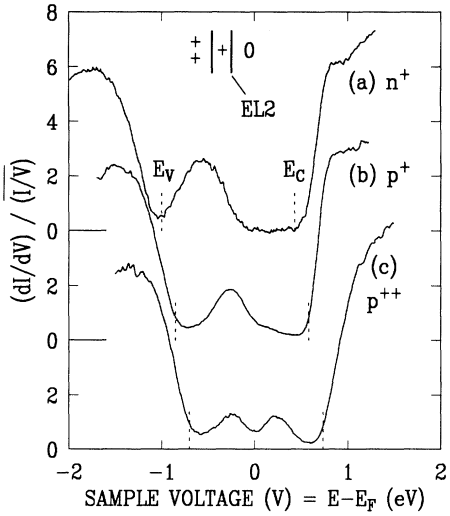

FIG. 1. Tunneling spectra acquired from layers of LT GaAs containing varying amounts of compensating shallow dopants. The valence-band maximum (E_v) and conduction-band minimum (E_c) are indicated by dashed lines in each spectrum. An intense band of states, arising from arsenic-related defects, appears within the band gap. The states of a bulk arsenic antisite defect are shown in the upper part of the figure, relative to the band edges of spectrum (a).

known $EL2$ level) [6], as shown in the top of Fig. 1 relative to the band edges of spectrum (a). The width of the band we interpret as arising from Coulomb interactions between neighboring arsenic-related defects (for a concentration of 1×10^{20} cm^{-3} their average separation is 22 Å) and with the shallow dopants [7]. Moving to Figs. 1(b) and 1(c), we see that as shallow acceptors are introduced into the material the Fermi level moves into the band of deep defect states. Thus, these states are donors. For spectrum (c), in which the Fermi level is roughly in the middle of the deep defect band, a distinct minimum in conductance forms at the Fermi level, indicating a gap of about 0.4 eV in the state density. We interpret this gap as arising primarily from the Hubbard U term (0.21 eV in the bulk) [8] separating the two donor levels of the antisite defect, although contributions from the Coulomb gap of the impurity band (0.1 eV in the bulk) [7] may also be present.

In Fig. 2 we show STM images of the p^+ LT-GaAs layer. These images are acquired with negative sample bias, so that the background atomic corrugation arises from the As sublattice of the GaAs. Numerous defects are visible in the images, and these defects can be classified into several types as labeled in Fig. 2. The largest apparent defect is type A, and the next largest is type B. Note the presence of two distinct satellites around the type B defects, and these satellites can be faintly seen around the type A defects as well. Other smaller types of defects are labeled C and D in Fig. 2, and most unlabeled defects in the images can be seen to fall within one of

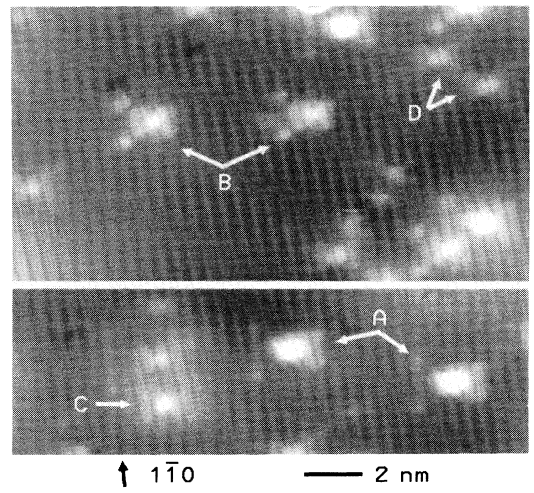

FIG. 2. STM images of the (110) cleaved surface of LT GaAs, acquired with 0.1 nA tunnel current and at a sample voltage of −2.0 V. Various point defects can be seen, and they are classified as types A, B, C, and D as indicated.

these four classes. Images such as those shown in Fig. 2 have been obtained from five samples with various shallow dopant concentrations, each with different probe-tip geometries, and the results for observed defect types and the presence of the satellite features have been reproduced in each case. It is important to note that for imaging of filled states near the band edge as in Fig. 2, the appearance of the defects is completely dominated by tunneling through the deep defect states. Voltage-dependent imaging of the empty states, which do not include contributions from the gap states, reveals a relatively unperturbed Ga sublattice in the vicinity of the defects, as shown in Fig. 3. Thus, the defect images shown in Fig. 2 are, in essence, images of the deep defect states seen in the spectra of Fig. 1.

In Fig. 4 we show expanded views of each of the types of defects observed in Fig. 2. A clue to the origin of the different types of defects can be obtained by noting the

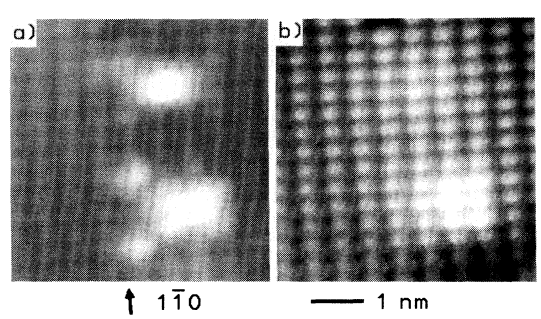

FIG. 3. STM image of identical surface regions, acquired at sample voltages of (a) −2.0 and (b) +2.0 V. Defects of type B and C are seen.

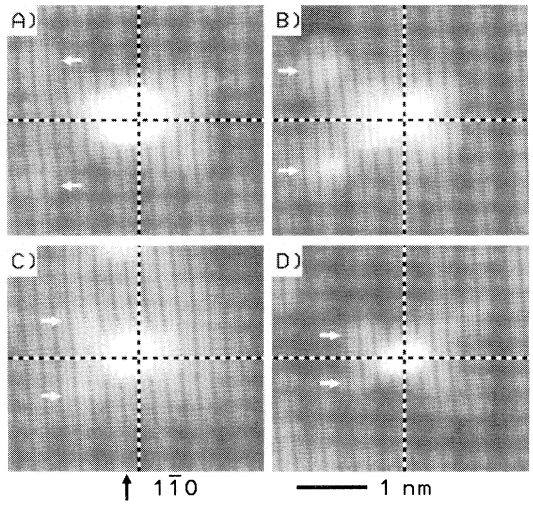

FIG. 4. Expanded view of the defect images type *A*, *B*, *C*, and *D*. The cross hairs in the images are located on the Ga sublattice (corrugation minimum) in (a) and (c), and on the As sublattice (corrugation maximum) in (b) and (d), in accordance with the model described in the text.

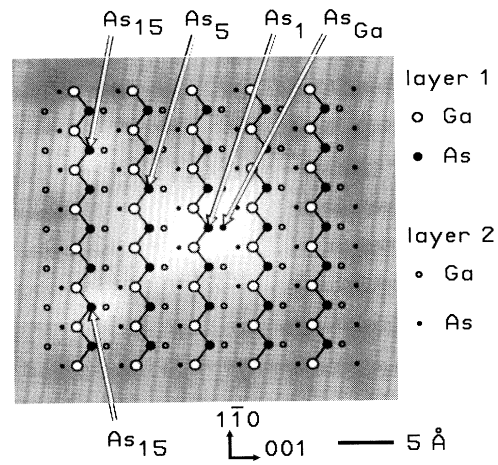

FIG. 5. Geometric model for the structure of the observed defect. Ga and As atoms in the first and second layers below the (110) surface are shown. An antisite defect (As_{Ga}) is located in the second layer. Arsenic atoms in several shells are labeled, with the observed satellite features corresponding approximately to the location of the 15th-nearest-neighbor (As_{15}) arsenic atoms located 15.2 Å from the antisite. The satellites are located along [1$\bar{1}\bar{2}$] and [$\bar{1}$1$\bar{2}$] directions relative to the defect one.

symmetry of the defects relative to the background As sublattice. In particular, the type *A* defects are seen to extend over an *even* number of rows in the [1$\bar{1}$0] surface direction [e.g., six rows between and including the satellites as indicated by the arrows in Fig. 4(a)], whereas the type *B* defects extend over an *odd* number of rows [five rows between and including the satellites as in Fig. 4(b)]. Similarly, the type *C* and *D* defects extend over an even and odd number of rows, respectively (satellites are not seen for these defects due to insufficient sensitivity, so the arrows in Fig. 4 simply mark the neighboring unit cells around the defect core). This type of even-odd symmetry is precisely what occurs for a defect on a given lattice site as one moves through consecutive higher-lying planes in the (110) direction. Thus, we interpret all of the observed images as arising from a single type of defect structure in which the defect core is located in differing lattice planes relative to the cleavage plane. This variation is, of course, to be expected for the present case of *bulk* defects in the GaAs. Specifically, the image types *A*, *B*, *C*, and *D* are interpreted as an arsenic-related point defect located 0, 1, 2, or 3 planes (2.0 Å spacing) below the (110) cleavage plane. From the observed structure of the type *A* images, the central core of the arsenic-related defect is seen to reside on the Ga sublattice.

Given the above interpretation of the images in terms of the depth of the defect core below the cleavage plane, we can construct a geometric model for the defect structure, as shown in Fig. 5. As a reference we choose the observed type *B* image, so that the defect core is in the second layer below the surface. Since the dominant defect in LT GaAs is known to be the arsenic antisite, and the location of this defect on the Ga sublattice is consistent with our observations, we place the antisite, As_{Ga}, in the second layer as shown in Fig. 5. All the defects observed here possess a single (1$\bar{1}$0) mirror plane passing through the central As_{Ga}, as shown by the horizontal dashed lines in Fig. 4. This is the only symmetry operation present on the (110) surface. If the defects themselves have lower than tetrahedral symmetry, then, assuming they are randomly oriented relative to the surface, a fraction of the observed defects should violate this (1$\bar{1}$0) mirror reflection. Even if the defects tend to orient themselves relative to the cleavage plane, we expect for defect complexes with low symmetry that the cleavage procedure will split some of the complexes, leading to a greater diversity of images and spectroscopy than that seen here. We conclude that the defects have tetrahedral symmetry in the bulk.

With the central core of the arsenic-related defects consisting of As_{Ga}, the outstanding question concerning the STM images is the origin of the observed satellites. This is of particular interest for these defects which are responsible for the *EL*2 level, since they are known to contain a central As_{Ga}, but considerable controversy surrounds the possibility of additional defects such as interstitial arsenic being located near the antisite defect [8–10]. The possibility that the observed satellites arise from two (or more) additional defects can be excluded on the basis of spatially resolved spectroscopy measurements: Current images acquired at voltages throughout the band gap reveal that the spectrum of states measured over the satellites is basically the same as that acquired over the defect core [11]. Thus, we conclude that the ob-

served satellite features are purely electronic features of the defect, arising from tails of the antisite wave function. The observed amplitude of the satellites corresponds to less than 1% of the state-density relative to that at the defect core. The satellite features probably arise from strain-related variations in surface buckling. Similar effects, though not so long range, have been seen in recent computations for Si donors at the GaAs(110) surface [12].

In conclusion, we have used the STM to study the geometric and electronic properties of arsenic-related point defects in LT GaAs. We observe a band of donor states located near $E_v+0.5$ eV arising from the defects, which is close to the energy of the well-known $EL2$ level in GaAs. The number of observed defects is about 1×10^{20} cm^{-3}, which is the same as the number of $EL2$-producing defects observed in LT GaAs by infrared adsorption studies [2]. We thus identify our defects as being identical to those which produce $EL2$ in LT GaAs, the structure which is known to consist primarily of an arsenic antisite [2,8–10]. We find a structure for the defect which is consistent with an isolated antisite in a tetrahedral environment. The possibility of a low symmetry defect complex, in particular an additional arsenic interstitial atom located along a [111] direction [9], is inconsistent with the observed symmetry and spectroscopy of our defects. A more complete understanding of the long range satellite features seen in the STM images may yield additional structural information concerning this $EL2$-producing defect.

We thank J. A. Stroscio and H. W. M. Salemink for discussions concerning STM probe-tip preparation and cross-sectional imaging.

[1] G. Cox, D. Szynka, U. Poppe, K. H. Graf, K. Urban, C. Kisielowski-Kemmerich, J. Krüger, and H. Alexander, Phys. Rev. Lett. **64**, 2402 (1990).

[2] See, e.g., M. Kaminska and E. R. Weber, Mater. Sci. Forum **83-87**, 1033 (1992), and references therein.

[3] H. W. M. Salemink, O. Albrektsen, and P. Koenraad, Phys. Rev. B **45**, 6946 (1992).

[4] R. M. Feenstra, E. T. Yu, J. M. Woodall, P. D. Kirchner, C. L. Lin, and G. D. Pettit, Appl. Phys. Lett. **61**, 795 (1992).

[5] A. Vaterlaus, R. M. Feenstra, P. D. Kirchner, J. M. Woodall, and G. D. Pettit, J. Vac. Sci. Technol. B (to be published).

[6] E. R. Weber, H. Ennen, U. Kaufman, J. Windscheif, J. Schneider, and T. Wosinski, J. Appl. Phys. **53**, 6140 (1982).

[7] B. I. Shklovskii and A. L. Efros, *Electronic Properties of Doped Semiconductors* (Springer-Verlag, Berlin, 1984). The energy scale for Coulomb interactions is $e^2N^{1/3}/\varepsilon=0.052$ eV for our system with dielectric constant of $\varepsilon=12.9$ and defect concentration of $N=1\times10^{20}$ cm^{-3}. The Coulomb gap is typically twice this value.

[8] J. Dabrowski and M. Scheffler, Phys. Rev. B **40**, 10 391 (1989).

[9] B. K. Meyer, D. M. Hofmann, J. R. Niklas, and J.-M. Spaeth, Phys. Rev. B **36**, 1332 (1987).

[10] M. K. Nissen, A. Villemaire, and M. L. W. Thewalt, Phys. Rev. Lett. **67**, 112 (1991).

[11] R. M. Feenstra, J. M. Woodall, and G. D. Pettit (to be published).

[12] J. Wang, T. A. Arias, J. D. Joannopoulos, G. W. Turner, and O. L. Alerhand, Phys. Rev. B **47**, 10 326 (1993).

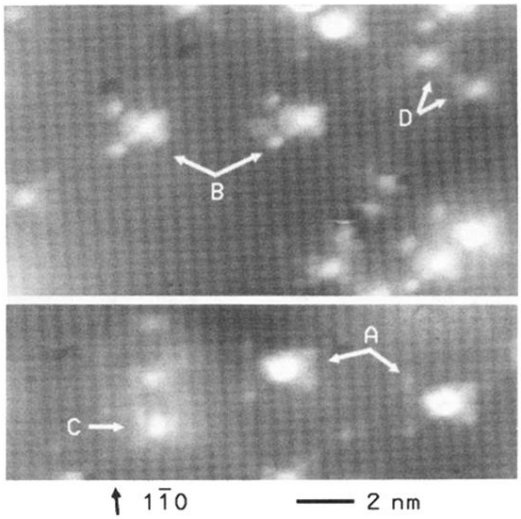

FIG. 2. STM images of the (110) cleaved surface of LT GaAs, acquired with 0.1 nA tunnel current and at a sample voltage of −2.0 V. Various point defects can be seen, and they are classified as types *A*, *B*, *C*, and *D* as indicated.

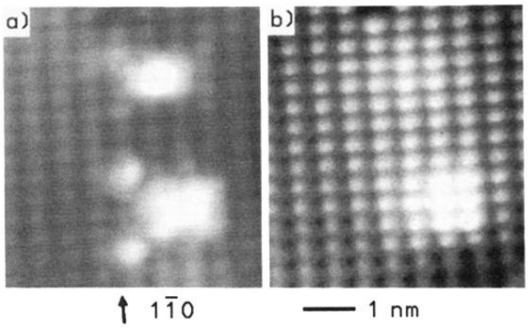

FIG. 3. STM image of identical surface regions, acquired at sample voltages of (a) −2.0 and (b) +2.0 V. Defects of type *B* and *C* are seen.

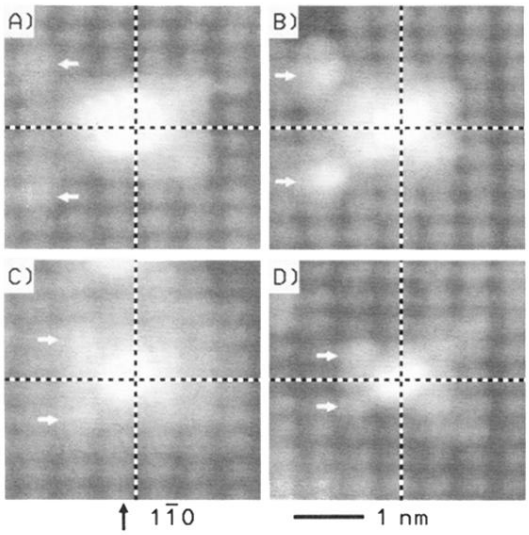

FIG. 4. Expanded view of the defect images type *A*, *B*, *C*, and *D*. The cross hairs in the images are located on the Ga sublattice (corrugation minimum) in (a) and (c), and on the As sublattice (corrugation maximum) in (b) and (d), in accordance with the model described in the text.

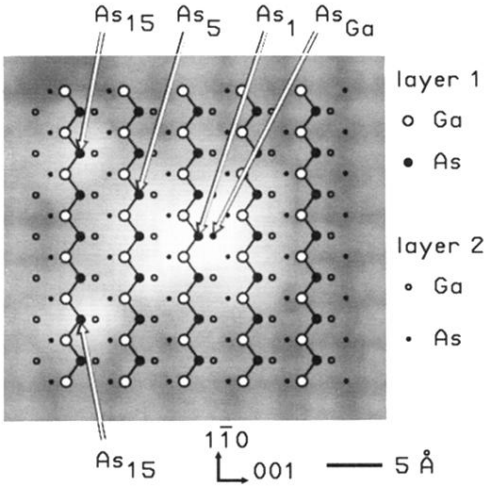

FIG. 5. Geometric model for the structure of the observed defect. Ga and As atoms in the first and second layers below the (110) surface are shown. An antisite defect (As_{Ga}) is located in the second layer. Arsenic atoms in several shells are labeled, with the observed satellite features corresponding approximately to the location of the 15th-nearest-neighbor (As_{15}) arsenic atoms located 15.2 Å from the antisite. The satellites are located along $[1\bar{1}\bar{2}]$ and $[\bar{1}1\bar{2}]$ directions relative to the defect one.